OES25-054

Early detection and monitoring of large scale hazardous substances spill from offshore platforms using autonomous underwater vehicle

Mahdi	CHOYEKH	Dept. Naval Architecture and Ocean Engineering, Osaka University mahdi@ naoe.eng.osaka-u.ac.jp
Naomi	KATO	Osaka University
Timothy	SHORT	SRI International
Yasuaki	YAMAGUCHI	Osaka University
Ryan	DEWANTARA	Osaka University
Muneo	YOSHIE	Port and Airport Research Institute
Toshinari	TANAKA	Port and Airport Research Institute
Eiichi	KOBAYASHI	Kobe University
Hajime	CHIBA	Toyama National College of Technology

Abstract

Oil spills caused by accidents of oil tankers and blowouts of oil and gas from offshore platforms cause tremendous damage to the environment as well as to marine and human life. Given the enormous impact oil spills, it is important provide tools in the battle against the consequences of oil spills and related natural pollution events. Particularly, AUVs can play an important role in detecting and surveying of such spills, as well as providing valuable information in order to mitigate the effects. In this context, an oil spill and blowout gas surveying AUV, called SOTAB-I, is being developed. In this paper, a general outline as well as the characteristics of SOTAB-I are presented. The experiment results obtained during the at-sea experiments demonstrated several surveying abilities of SOTAB-I. The robot managed to survey the dissolution of chemicals substances, such as methane gas. In addition, it could collect oceanographic data like water column distribution of temperature, salinity, and density. Furthermore, a high-resolution water current profile was obtainable.

INTRODUCTION

The world economy depends to a large extent on the use of energy. In order to meet the increasing need for energy, both in industry and daily life, petroleum activities, such as drilling and shipping, are on the rise. That requires additional attention to avoid accidents that can happen due to such activities. Oil spills and blowouts of oil and gas from the seabed cause serious damage to the environment as well as to the economy, not to mention the damage to marine and human life. In the case where methane gas is blown out from a seabed, it is partly dissolved in seawater then partly consumed by methanotrophs (Kessler et al., 2011), which leads to the creation of local hypoxia zones caused by oxygen depletion (Shaffer et al., 2009). The rest of the gas is released to the atmosphere, contributing to global warming, as methane is a highly potential greenhouse gas (Solomon et al., 2009).

Recently, several oil spill accidents have happened. Deepwater Horizon in the Gulf of Mexico in 2010 and the Elgin gas platform in the North Sea in 2012 are examples of these accidents. To prevent oil and gas spills from spreading and causing further damage to the environment over time, early detection and monitoring systems can be deployed around the offshore oil and gas production system. In addition, oceanographic data should be collected in order to comprehend the environmental changes around the accident. Based on the collected data, oil and gas drifting simulations must be performed to predict where the spilled oil will wash ashore and to adequately deploy oil recovery machines before this occurs.

SOTAB-I is a part of the SOTAB project (Choyekh et al., 2013), which has the following objectives: (1) autonomous tracking and monitoring of spilled plumes of oil and gas from subsea production facilities by an underwater AUV, (2) autonomous tracking of spilled oil on the sea surface and transmission of useful data to a land station through satellites in real time by multiple floating buoy robots (Senga et al., 2012), and (3) improvement of the accuracy of simulations for predicting diffusion and drifting of spilled oil and gas by incorporating real-time data (Takagi et al., 2012; Tsutsukawa et al., 2012).

There exists a wide variety of methods that deal with oil spills, and each presents strengths and weaknesses according to the circumstances and the purposes for which it is deployed. For substance dissolution measurement, the most commonly used technique is to extract discrete samples for subsequent

analyses (Joye et al., 2011). However, this method has limited temporal and spatial resolution. In addition, it requires much effort and is time consuming. Furthermore, there is a risk that the characteristics of the original collected samples could change during the collecting and handling processes. Other techniques are utilized to track a particular substance, such as oxygen, methane, or carbon dioxide. They can provide continuous information regarding the dissolution of substances but only for a particular and limited variety of substances. The Spilled Oil and gas Tracking Autonomous Buoy system (SOTAB-I) integrates an underwater mass spectrometer (UMS) that overcomes the previously mentioned weaknesses. The UMS enables real-time on site measurements with a high frequency. It is distinguished by its flexibility and good sensitivity as well as its reliability. It is able to detect multiple substance dissolutions simultaneously (Short et al., 2006).

The challenge in water surveying is not only to detect oil and substances dissolved in seawater, but also to obtain other related oceanographic data, as many research efforts have demonstrated that temperature (Servio et al., 2002), pressure (Handa, 1990), and salinity (Yang et al., 2007) are very important factors that considerably affect the formation and dissociation of gas hydrate. In addition, measurement of underwater currents is important for detecting and tracking dissolved gases and for predicting the evolution of the blowout gas in simulation models. There are few existing compact systems that are able to conduct a complete survey that can measure salinity, temperature, and depth in addition to underwater currents and dissolved gases simultaneously. SOTAB-I combines necessary sensors for a full and complete real-time and on site survey by integrating a UMS, an acoustic Doppler current profiler (ADCP), a conductivity-temperature-depth profiler (CTD), and a camera.

The development of a new type of AUV requires an evaluation process from two aspects. One is the guidance and control of the vehicle, and the other is the data sampling. This paper focuses mainly on the latter aspect. In the first part of this paper, a description of the underwater robot SOTAB-I and its characteristics are detailed. In the second chapter, oceanographic data collected at Toyama bay experiments are presented. The last chapter demonstrates the surveying abilities of the dissolution of chemical substances in the Gulf of Mexico in the USA.

1. OUTLINE OF SOTAB-I

A global overview of SOTAB-I is illustrated in Fig. 1. SOTAB-I is 2.3m length and it weighs 325Kg. It can be submerged in water as deep as 1500 meters. It can descend and ascend by adjusting its buoyancy through the buoyancy control device while changing its orientation, which is performed through two pairs of rotational fins. Robot can also move in the horizontal and vertical directions through two couples of horizontal and vertical thrusters. To know robot motion a compass and three axis rate sensors are used. When the robot is underwater, real time communication with the ship and robot tracking are ensured respectively through an acoustic modem and an acoustic navigation system (USBL). On the sea surface, an Iridium satellite communication transceiver module and a Global Positioning System (GPS) receiver are used for that purpose. SOTAB-I is also equipped with an Underwater Mass Spectrometer (UMS) in order to determine the characteristics and physical properties of dissolved gas and oil. It can measure at once the mass ratios ranging from 1 to 200 of the substances including dissolved gas and oil components. An Acoustic Doppler Current Profile (ADCP) is used to measure the magnitude and orientation of the underwater currents, and the Doppler Velocity Log (DVL) determines the altitude of the robot from seabed. In order to have a visual representation of gas blowout and oil plumes in addition to oil rig status, the robot was equipped with a camera and a stroboscope.

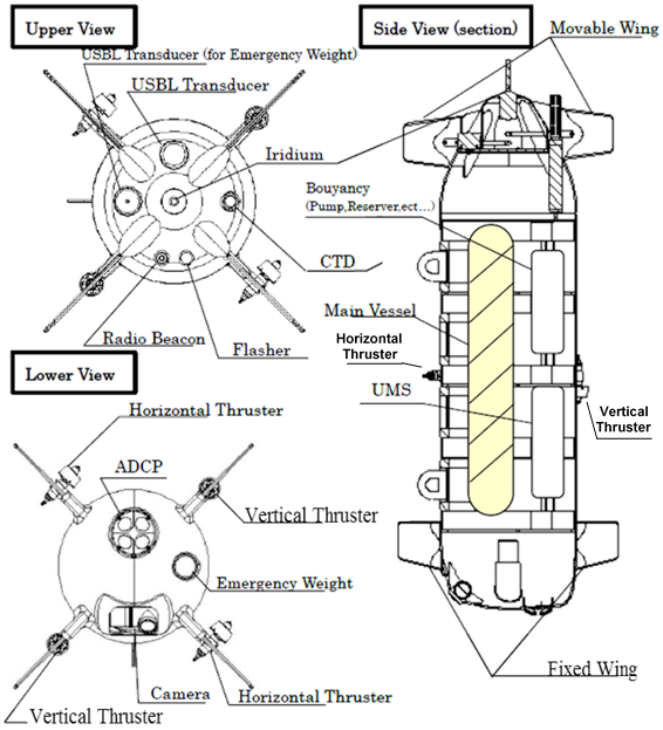

Fig. 1 Arrangement of devices and sensors installed on SOTAB-I.

SOTAB-I has four main surveying modes. The first is the water column survey mode in which the SOTAB-I moves along the water column by adjusting its buoyancy. The second mode is the rough guidance mode. It is used to collect rough data on physical and chemical characteristics of plumes by repeatedly descending and ascending on an imaginary circular cylinder centered at the blowout position of the oil and gas through the control of buoyancy and movable wings' angles. In the case where the UMS detects a high concentration of any particular substance, the third mode, which is the precise guidance mode, will be carried out to track and survey its detailed characteristics by repeatedly descending and ascending within the plumes. The fourth mode is the photograph mode, which enables us to have a large visual overview of the area around the blowout position of the oil and gas by taking pictures of the seabed. The SOTAB-I moves laterally using horizontal thrusters along a set route consisting of parallel straight lines to make mosaic images centered at the blowout position of the oil and gas.

In the following section, the water column survey mode will be the focus. Depth control is done using the buoyancy control device, which consumes less power than using perpendicular thrusters. Avoiding the use of thrusters in this mode will also help to not disturb the surrounding water during ADCP measurement of water currents.

2. SURVEY OF OCEANOGRAPHIC DATA

At-sea experiments were conducted in Toyama bay on the 20th of March 2015. Fig 10 on the left shows the mother ship "Sazanami", which belongs to Toyama National College University of Technology. The picture on the right shows the deployment of SOTAB-I in the seawater. The oceanographic data presented in this section were taken during a dive up to 220m.

Fig. 2 At-sea experiments in Toyama Bay

3.1 Water Column Distribution of Temperature, Salinity and Density

SBE-49 FastCAT from Sea-bird Electronics was the CTD sensor employed to measure conductivity, temperature as well as pressure. The sampling time was set to 1s. Table 1 summarizes the main characteristics of the CTD sensor employed.

Table 1 Main characteristics of the CTD sensor of SOTAB-I

Reference	CTD Sensor SBE-49 FastCAT
Constructor	Sea-bird Electronics
Range	Temperature: -5 to +35 °C Conductivity: 0 to 9 S/m Pressure: 0 to 7000 meters
Resolution	Temperature: 0.0001 °C Conductivity: 0.00005 S/m in oceanic waters Pressure 0.002% of full scale range

Based on CTD measurements, it is possible to calculate the depth, salinity, the density and the speed of sound. Table 2 summarizes oceanographic data that can be obtained with the CTD sensor with their associated symbols and scales.

Table 2 CTD related oceanographic data

	Symbol	Unit	Comment
Temperature	T90	[°C]	Given in ITS- 90 scale
Conductivity	C	[S/m]	
Pressure	P	[dcb]	
Depth	D	[m]	
Salinity	S	[ ]	Given in practical salinity scale PSS-78
Density	ρ	[kg/m3]	Based on the equation of state for seawater - EOS80

Fig. 3 shows results of data calculated based on CTD sensor measurements. Formulas for the computation of depth, salinity and density were obtained from (Fofonoff et Millard, 1983).

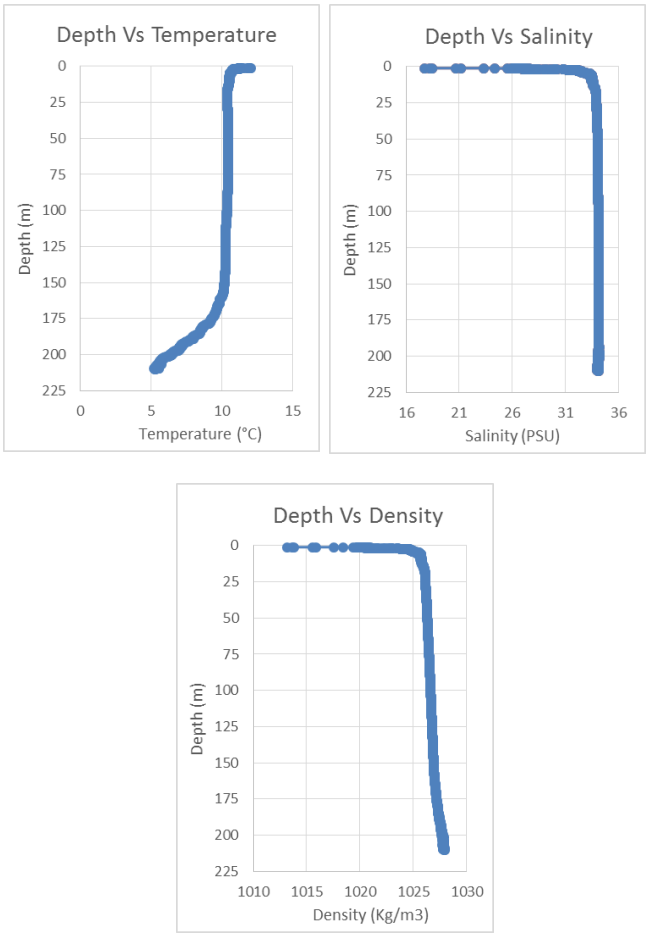

Fig. 3 Vertical distributions of temperature and salinity
(a) Temperature (b) Salinity (c) Density.

3.2 Water Column Profile of Water Currents

(1) ADCP configuration and characteristics

The Navigator WHN1200 from RD Instruments was used for water profiling and bottom tracking. The device integrates heading and attitude sensors necessary for coordinate's transformation. The accuracy of the compass is within +/-2° and attitude sensor is within +/- 0.5°. An integrated thermistor measures water temperature serves to improve the accuracy of calculation of sound speed and then, enhances the accuracy of the acoustic measurements. The device is mounted looking downwards at the bottom of the robot. The device has four beams with standard acoustic frequency FS equal to 1228.8 kHz enables high resolution measurements of water currents up to 15m range. Table 3 summarizes the main characteristics of SOTAB-I ADCP.

Table 3 SOTAB-I ADCP characteristics

Reference	Navigator WHN1200
Constructor	RD Instruments
System Frequency	1228.8 kHz
Beam pattern	Convex Sensor
Beam Angle	30 Degrees
Beam orientation	DOWN
Number of Beams	4
Range	≈15m

Robot Processor connects to ADCP/DVL device through RS232 serial port. The selected output format is PD0, which is a binary format that provides the most possible information. A virtual serial splitter serves to duplicate serial data input. One is directed to a serial logger software in order to save data in a file for ulterior detailed analysis. The other is input to the main program for real time processing of water currents and bottom tracking data.

SOTAB-I configuration was set as water profiling is done every second for 10 water layers referred also as bins with 0.5m thickness. Measurements are configured to be given in the Earth coordinates taking in consideration tilting and bin mapping. Most important characteristics and configuration are summarized in Table 4.

Table 4 SOTAB-I ADCP configuration

ADCP Configuration	Symbol	Value
Sampling Time	TE	1s
Pings/Ensemble	WP	1
Nb. of Depth Cells	WN	10
Layer thickness	WS	0.5 m
Water profiling Mode	WM	1
Blank after Transmit	WF	0.44 m
Salinity	ES	35
Depth of transducer	ED	0 m
1st Bin distance		0.99 m
Coordinate transformation	EX	0x1F (Earth coordinates, use tilts, 3-beam solutions, bin mapping)

The ADCP is installed in the top bottom of the body. Data of water current are collected when the robot is descending in order to reduce the turbulences that are induced by robot body motion.

(2) Water Current Profiling Process

Fig. 4 shows the steps needed for establishing water currents profile:

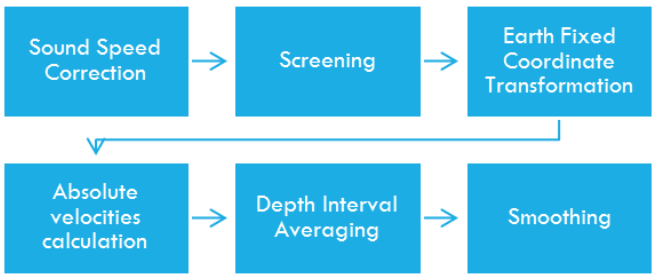

Fig. 4 Water Current Measurement Process

- *Sound speed correction*

The accuracy of velocities in any coordinate system is directly connected to sound speed: an error of 1% in sound speed will result in 1% error in velocity measurement. The sound speed in seawater depends on pressure, temperature and salinity. The WHN120 integrates a thermistor able to measure temperature but it is not equipped with any pressure or salinity sensors. The ADCP calculates sound speed based on the measured temperature and pre-set salinity. However, salinity of seawater is variable especially near the sea surface. In order to obtain accurate velocity data, the ADCP needs to know the real speed of sound in water. For that reason, sound speed near the transducer is calculated based on the CTD sensor measurements.

It is possible to correct velocity data in post processing by using the following equation:

$$V_{CORRECTED} = V_{UNCORRECTED} (C_{REAL} / C_{ADCP}) \quad (1)$$

Where CREAL is the real sound speed at the transducer, and CADCP is the speed of sound used by the ADCP.

Ranges of cells, to a smaller extent, are also affected by sound speed variations and then are subject to correction. Range may be corrected by using the following equation:

$$L_{CORRECTED} = L_{UNCORRECTED} (C_{REAL} / C_{ADCP}) \quad (2)$$

Where

$L_{CORRECTED}$: Corrected range cell location

$L_{UNCORRECTED}$: Uncorrected range cell location

- *Screening*

This step is performed automatically by the ADCP. Velocity data are subject to four kinds of screening: the correlation test, the fish rejection algorithm, the error velocity test, and the percent good test. At this stage, the ADCP checks the reasonableness of the velocity components for each depth cell and flags bad data.

- *Transformation to Earth fixed coordinates*

At first stage, the ADCP transforms vector of beam velocities to the vector of velocity components in the instrument fixed coordinate system. The ADCP was configured to convert the data to Earth coordinates (East, North, Up) based on tilt and heading data.

- *Calculation of absolute velocity*

The robot speed VSOTAB-I should be added to the measured relative water current velocity VADCP in order to obtain the absolute velocity V of water currents. V can be obtained using the following equation:

$$V = V_{ADCP} + V_{SOTAB-I} \quad (3)$$

SOTAB-I can provide robot velocities either from the DVL when bottom tracking is active or from USBL positioning system.

- *Depth interval averaging*

When the robot is descending along the water column, water profile of ADCP depth cells overlap giving multiple measurements for each water depth. Having high density of measurements helps to reduce random errors. Following, we will refer to ADCP depth cells by “bins” in order to differentiate it from the depth cells of water column. Each ADCP bin measures water current at its corresponding depth. At first step, it is important to calculate the corrected depth associated with each bin (Bin_{iDepth}) given by

$$Bin_{iDepth} = D_{CTD} + D_0 + Bin_{1Dist} + WS * (Bin_i - 1) \quad (4)$$

Where D_{CTD} is the depth value calculated based on CTD sensor pressure data, D_0 is the distance between the CTD sensor and the ADCP, WS is the bin thickness defined in Table 4 and Bin_{1Dist} is the distance to the middle of the first bin. The previous equation doesn’t take in the consideration

the tilt angle θ of the robot from the vertical axis. For that reason solution obtained in equation should be multiplied by cos θ. θ can be estimated from the measured pitch p and roll r angles.

At second stage, after depths are corrected, depth and its associated velocity of all bins will be input to a depth interval velocity averaging program as showed in Fig. 5.

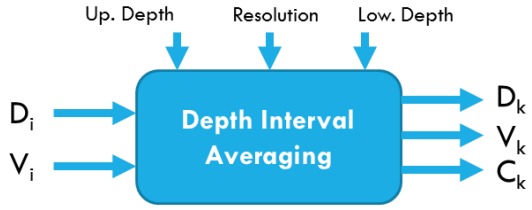

Fig. 5 Depth interval averaging program inputs and outputs

The water column will be divided into a number of depth layers DN with R resolution between a certain lower and upper depth. DN is calculated using the following formula

$$D_N = |\text{Upper Depth} - \text{Lower Depth}| * \text{Resolution} \quad (5)$$

Water velocities V_i at depth D_i will be averaged within D_N discrete depth intervals. For each depth interval D_k, average velocity value V_k with a certain coefficient C_k corresponding to the number of samples measured. For each depth layer, the program makes the sum of the water currents and then divide it by the number of samples measured within its range.

- *Smoothing*

In the previous step, we associated with each depth cell a coefficient that reflects the density of measurements at this depth. The number of samples will be the coefficient that will be associated to each depth layer when calculating the moving average

$$V_{iF} = \frac{\sum_{i+n/2}^{i-n/2}(V_i * C_i)}{\sum_{i+n/2}^{i-n/2} C_i} \quad (6)$$

Where n is the number of depth cell to be averaged

(3) Evaluation of ADCP Data

Fukae-maru was equipped with an ADCP Broadband 307.2 kHz configured to perform water profiling every minute for 40 water layers with 2m thickness. SOTAB-I configuration was set as water profiling is done every second for 10 water layers with 0.5m thickness. Main characteristics and configuration are summarized in Table 5.

Table 5 Characteristics and Settings of Fukae-maru ADCP

ADCP	FUKAE-MARU
Reference	RDI Broadband
Frequency	307.2kHz
Sampling Time	60s
Pings/Ensemble	23
Nb. of Layers	40
Layer thickness	2 m
Standard deviation	6.6 cm/s
Range	110m

Fig. 6 shows that water profile measured by SOTAB-I is in good agreement with Fukae-maru profile. Water current direction as well as its curve trend are very similar particularly in the North-South direction. The maximum shifting is around 10cm/s and was observed in the East-West direction. The differences may be explained by the temporal and spatial variation of SOTAB-I and Fukae-maru positions. In addition, water currents are varying over time. Finally, the resolution of the two compared ADCPs is different as SOTAB-I has better resolution enabling it to get high resolution profiling and higher density of measurements which contribute in the decrease of random errors.

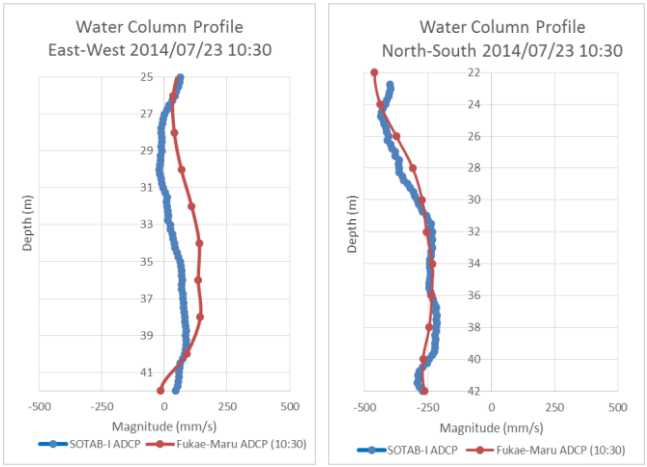

Fig. 6 Comparison between SOTAB-I and Fukae-maru ADCPs

(4) Water column profile at Toyama Bay

Fig. 7 shows the results of calculation of the water currents profile. It shows that the water currents flowing to the northwest direction was dominating.

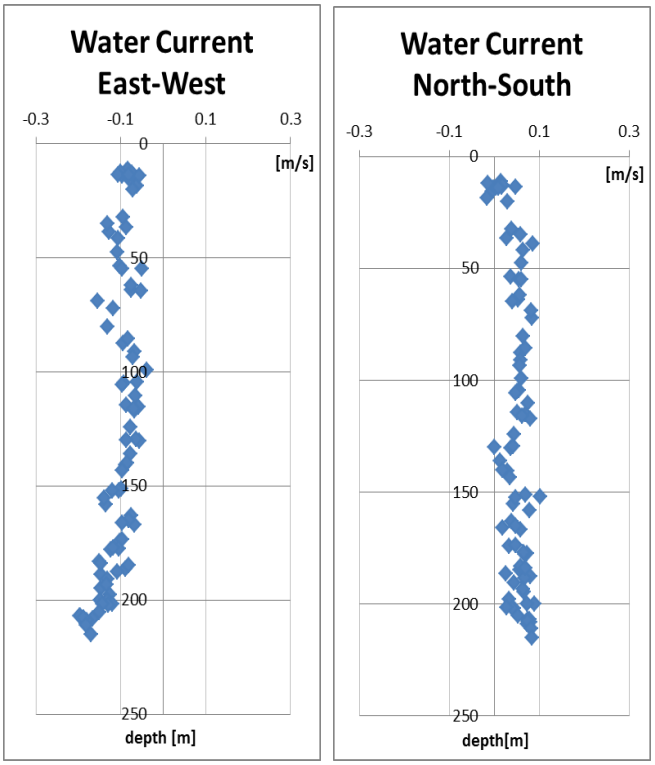

Fig. 7 Vertical profile of water currents (a) in the East-West direction, (b) in North - South direction

3. SURVEY OF DISSOLUTION OF CHEMICAL SUBSTANCES

At-sea experiments were performed from the 6th to the 15th of December 2013 in the Gulf of Mexico in the US (Fig. 8), near where the Deepwater Horizon oil spill accident in 2010 and the Hercules 265 oil rig blowout in 2013 occurred leading to the release of methane gas. Due to the strong wind and severe weather conditions, experiments were carried out in shallow water and in particular, at the mouth of the Mississippi River, where the UMS data were measured. The area is characterized by its prevalent abandoned oilrigs and natural seepage of hydrocarbons (Mitchell et al., 1999).

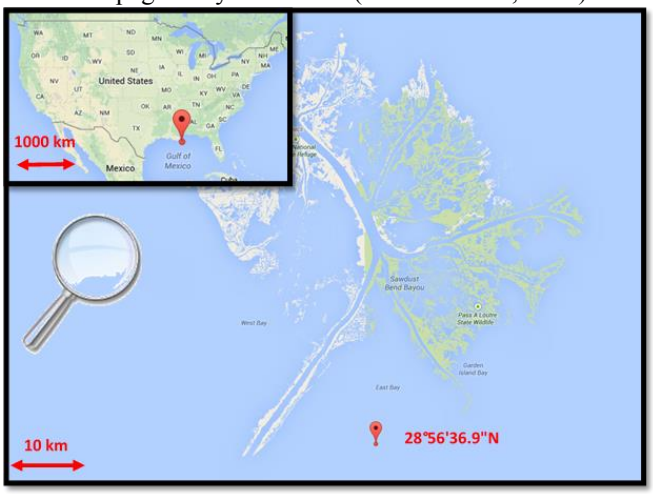

Fig. 8 Gulf of Mexico experimental zone (Google Map)

This section is mainly focuses on the measurement results of the dissolution of chemical substances obtained on the 13th of December 2013 from 13:30 to 14:30 dive.

The UMS instrument used for the SOTAB-1 deployments contained a 200 amu linear quadrupole mass analyzer (E3000, Inficon, Inc., Syracuse, New York). Table 6 provides the specifications of the Stanford Research Institute (SRI) membrane introduction mass spectrometry (MIMS) system.

Table 6 MIMS Specifications.

Mass Analyzer Type	Linear Quadrupole Mass Filter
Mass Range	1-200 amu
Inlet System	Membrane Introduction (PDMS)
Power Consumption	60 - 80 Watts
Operation Voltage	24 VDC
Maximum Deployment Time	10 -14 Days (exhaust limited)
Dimensions	Diameter 24 cm, Length 64 cm
Weight	35 kg
Depth Capability	2000 m

Introduction of analytes into the mass spectrometer occurs through a hydrophobic and nonporous high-pressure polydimethlyl siloxane (PDMS) membrane introduction system, pressure tested to a depth of 2,000 m. Water samples are placed in contact with the semi-permeable membrane, usually at a constant flow rate. The transport of dissolved gases and relatively non-polar volatile organic compounds (VOCs) through these membranes is compound-specific and temperature-dependent, but typically requires that the solute dissolves into the membrane, diffuses through it, and finally evaporates into the mass spectrometer. Once in the mass spectrometer vacuum chamber, the neutral gas-phase analytes are (1) ionized by electron impact, (2) sorted by their mass-to-charge (m/z) ratios (typically z = 1), and (3) detected to create a mass spectrum. The membrane interface used in this system provides parts-per-billion level detection of many VOCs and sub parts-per-million detection limits for many dissolved light stable gases.

The membrane probe assembly consists of a hollow fiber PDMS membrane stretched and mounted on a sintered Hastelloy C rod. One end of the supported membrane is capped with a polyetheretherketone (PEEK) rod; the other end is connected to the vacuum chamber via stainless steel tubing. The membrane assembly is inserted into a steel heater block that houses a thermocouple and heater cartridges for controlling sample and membrane temperature (+/- 0.1°C). A magnetic piston pump draws ambient water into the sample tubing, through the membrane probe assembly, and back to the environment.

The UMS was calibrated for dissolved gases (methane, nitrogen, oxygen, argon, and carbon dioxide) by equilibrating acidified artificial seawater for more than one hour with gas mixtures that contained certified mole fractions of the gases. Salinity and temperature, measured during sample analysis, allowed calculation of dissolved gas concentrations. Gas volume percentages are shown in Table 7. The UMS was calibrated for ethane, propane, and butane by equilibrating seawater with gas mixtures that contained a certified mole fraction of ethane, propane, or butane for two point calibrations of these gases (background and one concentration). The UMS was also calibrated for VOCs by analysis of VOC standards created by serial dilution of stock solutions of benzene, toluene, and xylenes. Calibration was not performed for hydrogen sulfide or naphthalene. Each sample was analyzed until a stable signal was achieved. Blank samples (i.e., UMS residual gas backgrounds) were measured by leaving deionized water in the MIMS assembly with the sample pump inactivated overnight to allow complete degassing of the sample in contact with the membrane. The UMS assembly temperature was controlled at 25°C during calibration to mimic deployment conditions. The UMS cast data were subsequently converted to concentrations for the dissolved gases (μmol/kg) and VOCs (ppb) from the calibration parameters and concurrently collected physical (CTD) data using algorithms and software developed by the Stanford Research Institute (SRI).

Table 7 Standard gas mixtures used for equilibration (in volume %).

Gas	Mixture 1	Mixture 2	Mixture 3	Mixture 4
Methane	0.0995	0.2500	2.5000	3.351
Nitrogen	Balance	Balance	Balance	Balance
Oxygen	20.85	21.0000	17.0100	9.9600
Argon	1.009	1.3010	1.0040	0.6990
Carbon Dioxide	0.0990	0.7510	0.1500	0.0400

Linear least squares regressions provided UMS calibration coefficients for methane, nitrogen, ethane, oxygen, propane, argon, carbon dioxide, and butane concentrations using measured UMS ion currents, at m/z of 15, 28, 30, 32, 39, 40, 44, and 58. The ion current at m/z 44 (called I44), which is the mass spectrometer ion signal intensity for m/z 44 corresponding to the diagnostic ion for carbon dioxide, was also used in the nitrogen regression to account for contributions from carbon dioxide fragmentation.

Additionally, all signal intensities were background corrected by subtracting the signal intensity at m/z 5 (electronic background); this subtraction accounts for changes in electronic noise resulting from UMS temperature variability. The signal intensity at m/z 5 is used as the electronic background because there is no chemical that will give a peak in the mass spectrum at m/z 5. The "argon" or "water" correction is then used, as described in (Bell et al., 2007; Bell, 2009), to account for temperature variations in the field. The UMS calibration parameters and deployment parameters were identical. The calibration parameters that were identical were the sample flow rate and temperature of the membrane introduction heater block. A time delay was applied to the UMS cast data to adjust for the sample travel time through the tubing and membrane permeation.

The argon and water vertical profiles are the measured ion intensities at m/z 40 (argon) and m/z 18 (water vapor) as a function of depth. These are used to normalize the concentration profiles of the other analytes to account for changes in permeation through the membrane interface with increased pressure, as well as other changing environmental conditions that affect the signal intensities (Bell et al. 2007; Bell, 2009), therefore, high frequency noise in these data sets was removed using a Butterworth filter prior to normalization of the other profiles.

The typical measurement accuracy at best is 2%, but this varies for different chemicals. The response time is at best 5-10 s for the light compounds and worse for the high molecular weight compounds. A typically reasonable spatial resolution can be obtained with an ascent and descent rate of 0.5 m/s. As mentioned in the robot maneuverability section, the maximum vertical and lateral speed of the SOTAB-I are below that rate.

Fig. 9 illustrates the change of concentration of some substances along the water column. Fig. 9 (a) and (b) show the vertical concentration profiles for nitrogen and argon needed for the calculation of the other substances dissolution profiles mentioned previously, respectively. Fig. 9 (c) demonstrates that the concentration of methane in the upper water layers is negligible down to a depth of 30 m, and that it starts to increase steadily down to a water depth of 44.6 m. In Fig. 9 (d), it can be observed that the oxygen concentration moderately decreased from a water depth of 0 m to that of 10 m, followed by slower rate of decline from of 10 m to 27 m water depth. Then, oxygen concentrations declined considerably from a water depth of 27 m to that of 44 m. It can be seen that the oxygen concentration decreased with increasing depth. In Fig. 9 (e), three zones can be distinguished based on the change in carbon dioxide concentrations: in water depths between 0 m and 10 m, carbon dioxide concentrations decreased gradually, from 10 m to 27 m water depths it kept decreasing but at a slower rate, and below 30 m, carbon dioxide concentrations increased down to a water depth of 44 m.

From this perspective, we can say that the SOTAB-I succeeded in measuring dissolved substance variations along the vertical water column. On the other hand, other alkanes and benzene-toluene-xylene (BTX) were below the sensory threshold and had no significant concentrations.

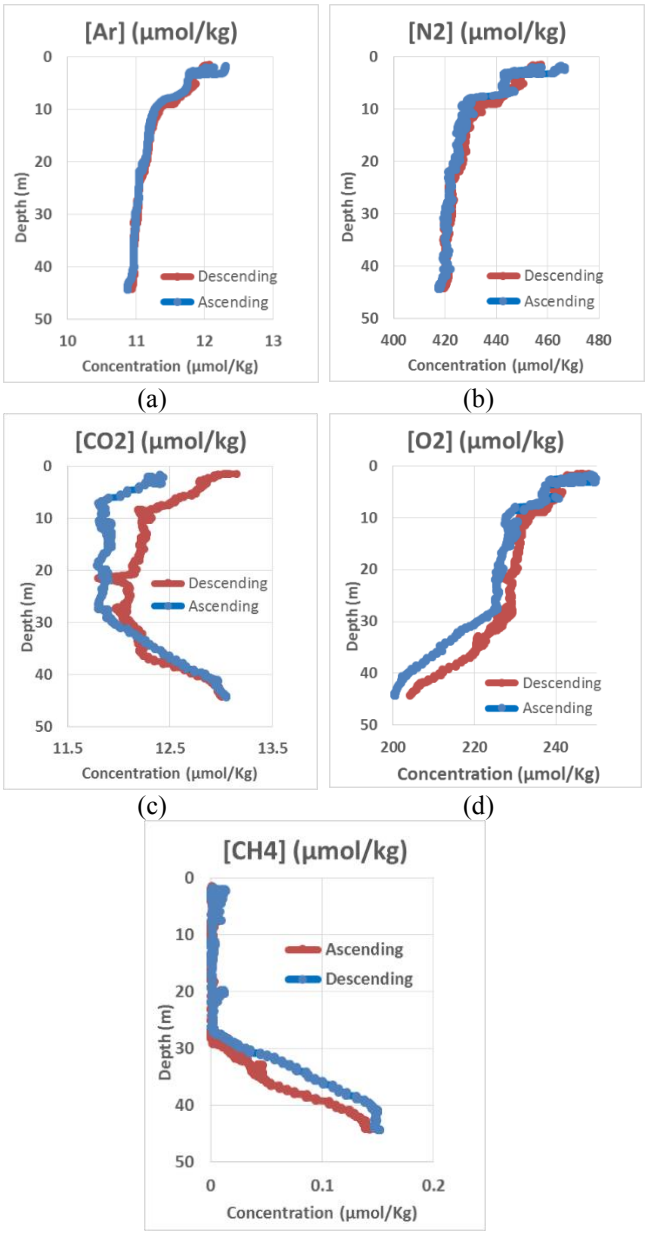

Fig. 9 Dissolution of substances in the water column
(a) Nitrogen (b) Argon (c) Carbon Dioxide (d) Oxygen
(e) Methane

There are very few methods to verify or corroborate the UMS measurements. We have used dissolved oxygen (DO) sensors in the past to compare the UMS oxygen measurements (m/z 32), and the comparison was generally very good (Bell et al., 2007; Bell, 2009). The SOTAB-1 deployments were not at a location where we would expect to see alkanes and BTX. We believe that the methane that we detected was biogenic methane and not associated with an oil reservoir. We have verified the UMS ability to detect these compounds in the lab and in other deployments (see Wenner et al., 2004 for BTX using an earlier version).

CONCLUSIONS

In order to prevent further damage caused by oil spills and gas blowout accidents, a spilled oil and gas tracking autonomous buoy system (SOTAB-I) is being developed. It has the advantages of being a compact system able to perform high resolution measurements. The robot can collect oceanographic data and transmit them in real time with their corresponding position, making it suitable for rapid inspection. Collected data will help to comprehend the environmental changes due to the accident and boost the accuracy of oil drifting simulation, which contributes to the efforts to avoid further damage that can be caused by oil spill disasters.

In this paper, the outline of SOTAB-I as well as its general characteristics and operational modes were described. Toyama Bay experiments were a good opportunity to demonstrate the ability of SOTAB-I to perform water column survey of oceanographic data. The water currents measurement process was established and evaluated. In the Gulf of Mexico experiments, SOTAB-I could survey the concentration of the chemical substances.

Survey efforts of the oceanographic data and the dissolution of substances need to be continued in order to extend the range not only in the vertical plane but also to cover a cylindrical area with the diameter of 5km as described in the rough mode. In the near future, in order to demonstrate the abilities of SOTAB-I in deep water, deployment of the robot is scheduled in water depth of 1000 m in Niigata in the Japan Sea where natural methane seepage was reported.

ACKNOWLEDGEMENTS

This research project is being funded for 2011FY-2015FY by Grant-in-Aid for (Scientific Research(S) of Japan Society for the Promotion of Science (No. 23226017).

REFERENCES

1) Bell, R. J. (2009). “Development and Deployment of an Underwater Mass Spectrometer for Quantitative Measurements of Dissolved Gases,” Ph.D. Thesis, University of South Florida, St. Petersburg, Florida.

2) Bell, R. J., Short, R. T., and Byrne, R. H. (2011). “In Situ Determination of Total Dissolved Inorganic Carbon by Underwater Membrane Introduction Mass Spectrometry,” Limnol. Oceanogr.-Meth, 9, 164-175. doi: 10.4319/lom.2011.9.164.

3) Bell, R. J., Short, R. T., Amerson, F. W. V., and Byrne, A. (2007). “Calibration of an In Situ Membrane Inlet Mass Spectrometer for Measurements of Dissolved Gases and Volatile Organics in Seawater,” Environ. Sci. Technol., 41, 8123–8128.

4) Choyekh, M., Kimura, R., Akamatsu, T., Kato, N., Senga, H., Suzuki, H., Okano, Y., Ban, T., Takagi, Y., Yoshie, M., Tanaka, T., and Sakagami, N. (2013). “Development of Spilled Oil and Gas Tracking and Monitoring Autonomous Buoy System and its Application to Marine Disaster Prevention,” *International Society of Offshore and Polar Engineers,* Anchorage, ISOPE, Vol.1, pp. 695-702.

5) Fofonoff, N., Millard, R. (1983). “Algorithms for computation of fundamental properties of seawater,” Unesco technical papers in marine science, #44, pp. 1-53.

6) Handa, Y. P. (1990). “Effect of hydrostatic pressure and salinity on the stability of gas hydrates,” J Phys Chem, 94: 2652-2657.

7) Joye, S. B., MacDonald, I. R., Leifer, I., and Asper, V. (2011). “Magnitude and oxidation potential of hydrocarbon gases released from the BP oil well blowout,” Nature Geoscience 4, pp. 160–164.

8) Kessler, J. D., Valentine, D. L., Redmond, M. C., Du, M., Chan, E. W., Mendes, S. D., Quiroz, E. W., Villanueva, C. J., Shusta, S. S., Werra, L. M., Yvon-Lewis, S. A., and Weber, T. C. (2011). “A Persistent Oxygen Anomaly Reveals the Fate of Spilled Methane in the Deep Gulf of Mexico,” Science 21, Vol. 331 no. 6015, pp. 312-315.

9) Mitchell, R., MacDonald, I. R., and Kvenvolden, K., (1999). “Estimates of total hydrocarbon seepage into the Gulf of Mexico based on satellite remote sensing images,” EOS Supplement 80, OS242.

10) Senga, H., Kato, N., Yu, L., Yoshie, M., and Tanaka, T. (2012). “Verification Experiments of Sail Control Effects on Tracking Oil Spill,” *OCEANS 2012,* Yeosu, IEEE, May 21-24, Proc. (CD-ROM).

11) Servio, P. and Englezons P. (2002). “Measurement of dissolved methane in water in equilibrium with its hydrate,” J Chem Engineer Data, 47:87-90.

12) Shaffer, G., Olsen, M. S., and Pedersen, J. O. P. (2009). “Long-term ocean oxygen depletion in response to carbon dioxide emissions from fossil fuels,” Nature Geoscience 2, 105–109.

13) Short, R. T., Toler, S. K., Kibelka, G. P. G., Rueda Roa, D. T. Bell, R.J., and Byrne, R.H. (2006). “Detection and quantification of chemical plumes using a portable underwater membrane introduction mass spectrometer,” Trends in Anal. Chem., 25 (7), 637–646.

14) Solomon, E. A., Kastner, M., MacDonald, I. R., and Leifer, I. (2009). “Considerable methane fluxes to the atmosphere from hydrocarbon seeps in the Gulf of Mexico,” Nature Geoscience 2, 561–565.

15) Takagi, Y., Ban, T., Okano, Y., Kunikane, S., Kawahara, S., Kato, N., and Ohgaki, K. (2012). “Numerical tracking of methane gas/hydrate and oil droplet in deep water spill,” *Proc. of InterAcademia 2012*.

16) Tsutsukawa, S., Suzuki, Y., and Kato, N. (2012). “Efficacy Evaluation of Data Assimilation for Simulation Method of Spilled Oil Drifting,” *Proc. of 5th PAAMES and AMEC2012,* Taiwan, Paper No. SEPAS-05

17) Wenner, P. G., Bell, R. J., Van Amerom, F. H. W., Toler, S. K., Edkins, J. E., Hall, M. L., Koehn, K., Short, R. T., and Byrne, R. H. (2004). “Environmental Chemical Mapping using an Underwater Mass Spectrometer”, TrAC, Trends Anal. Chem. 2004, 23, 288-295. doi:10.1016/S0165-9936(04)00404-2.

18) Yang, D. H., and Xu, W. Y. (2007). “Effects of salinity on methane gas hydrate system,” Sci China Ser D-Earth Sci, Vol. 50 | no. 11 | 1733-1745, Springer.